applied sciences

MDPI

Article

Analysis on Evaluations of Monterey Bay Aquarium Research Institute's Wave Energy Converter's Field Data Using WEC-Sim and Gazebo: A Simulation Tool Comparison

Chris Dizon [1], Ryan Coe [2], Andrew Hamilton [3], Dominic Forbush [2], Michael Anderson [3], Ted Brekken [1,*] and Giorgio Bacelli [2]

[1] Electrical Engineering and Computer Science, Oregon State University, Corvallis, OR 97331, USA; dizonc@oregonstate.edu
[2] Sandia National Laboratories, Albuquerque, NM 87123, USA; rcoe@sandia.gov (R.C.); dforbus@sandia.gov (D.F.); gbacell@sandia.gov (G.B.)
[3] Monterey Bay Aquarium Research Institute, Moss Landing, CA 95039, USA; hamilton@mbari.org (A.H.); anderson@mbari.org (M.A.)
* Correspondence: brekken@engr.oregonstate.edu

Abstract: Although many studies have validated wave energy converter (WEC) numerical models against scaled prototype experimental data, there remains a notable lack of validation using data from full-scale deployed WECs. This paper compares two numerical models of Monterey Bay Aquarium Research Institute's Wave Energy Converter (MBARI-WEC), a two-body point absorber with an electro-hydraulic power take-off system (PTO). The models are implemented in *WEC-Sim/Simscape* and *Gazebo Simulator*. A statistical analysis of the models was performed, and field results were obtained to compare the models' accuracy in predicting the RMS piston velocity, RMS motor speed, and mean electric power compared to field data for 56 observations across varying sea states. The *Gazebo* model demonstrated a closer agreement across all three parameters for a majority of the observations. When compared to the field data, the *Gazebo* and *WEC-Sim* models exhibited average mean electric power overestimations of 13% and 22%, respectively.

Keywords: software packages; statistical analysis; time-domain analysis; wave energy converters

check for updates

Citation: Dizon, C.; Coe, R.; Hamilton, A.; Forbush, D.; Anderson, M.; Brekken, T.; Bacelli, G. Analysis on Evaluations of Monterey Bay Aquarium Research Institute's Wave Energy Converter's Field Data Using WEC-Sim and Gazebo: A Simulation Tool Comparison. *Appl. Sci.* **2024**, *14*, 11169. https://doi.org/10.3390/app142311169

Academic Editor: José A. Orosa

Received: 2 October 2024
Revised: 13 November 2024
Accepted: 22 November 2024
Published: 29 November 2024

1. Introduction

Accurate numerical models of physical systems are vital resources for the design and optimization of complex systems. They aid in understanding the effects on the system before undergoing physical design changes or implementing ideas such as new control strategies. Although many studies have validated wave energy converter (WEC) numerical models against scaled prototype experimental data, there remains a notable lack of validation using data from full-scale deployed WECs. A summary of studies with WEC validation against numerical analyses, real sea data, and mooring systems is presented in [1], where the authors note that not only are there a limited number of WECs that have been deployed at full-scale, but the measured data from them are typically not publicly available. To address this gap, two numerical models have been developed that represent Monterey Bay Aquarium Research Institute's Wave Energy Converter, the *MBARI-WEC*, which has been operating for six-month periods since 2014 [2].

The MBARI-WEC is a two-body point absorber consisting of a surface buoy and a submerged heave cone connected together by an electro-hydraulic power take-off (PTO) system as shown in Figure 1. The relative heave motion between the surface buoy and heave cone actuates the PTO piston, driving a hydraulic motor directly coupled to an electric motor/generator. The electric power generated is transmitted to a battery or a load dump heater if the batteries cannot accept the power. Battery power can be utilized on-board for sensors, data acquisition, data logging, data transmission, and auxiliary systems.

An air spring provides a restoring force against the weight of the heave cone. The heave cone doors can open and close to alter the system's drag in the event of severe sea states. See [3] for further device description, as well as [4] for more details regarding the PTO design and operation.

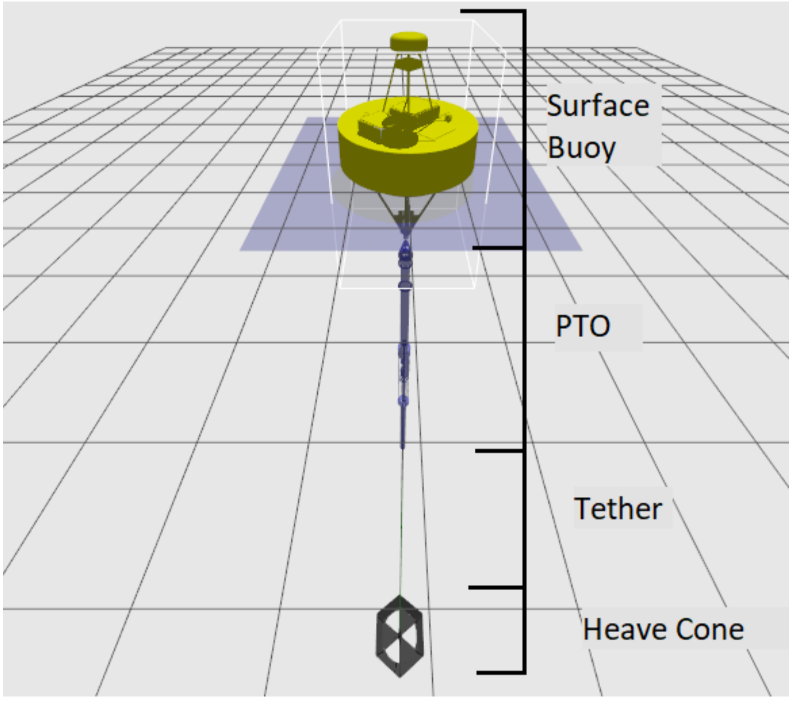

Figure 1. The MBARI-WEC portrayed in *Gazebo*. Labeled from top to bottom are the surface buoy, PTO, tether, and heave cone. Relative motion between the surface buoy and heave cone actuate the PTO piston which drives a hydraulic/electric motor. An air spring driven by the piston provides the necessary restoring force.

Two numerical models of the MBARI-WEC are considered in this study, and it is important to note that the fundamental nature of the two models are different, as described below. One model was created using *WEC-Sim*, Wave Energy Converter Simulator, utilizing Matlab, Simulink, and Simscape Multibody [5]. This model is a combination of two individual numerical models, the hydrodynamics and the PTO system, and is intended to serve as a component-based model of the MBARI-WEC as its inputs are derived from data or specifications of the physical system. A second numerical model for the MBARI-WEC was developed as a software interface project using the ROS 2 (Robotic Operating System) framework [6] and *Gazebo* as the simulation environment [7]. ROS 2 serves as the software platform in both the *Gazebo* model and the physical MBARI-WEC hardware, therefore using ROS 2 features in simulation is identical to coding interactions with the physical system. The *Gazebo* model is intended to be used as a digital twin of the MBARI-WEC, allowing users to work with the same interface as the real hardware and develop and test their work before deployment on the real system [2]. The goal of this paper was to analyze the accuracy of the *WEC-Sim* and *Gazebo* models when comparing the field data recorded by the MBARI-WEC to the outputs, thus providing insight into the trade-offs and benefits between the use of one model over the other. These parameters were obtained via a Sofar Spotter buoy and data being reported from the MBARI-WEC itself.

2. Materials and Methods

2.1. WEC-Sim and Gazebo Descriptions

The equations of motion for forces acting on a body as solved by both the *WEC-Sim* and *Gazebo* models can be expressed as:

$$m\ddot{X}(t) = F(t) \tag{1}$$

where m is the mass matrix, $\ddot{X}(t)$ the 6-degree-of-freedom (DOF) acceleration vector, and $F(t)$ are the 6-DOF total forces on the body. Both of these models represent hydrodynamic forces based on linear wave theory which assumes the fluid flow is inviscid, incompressible, and irrotational [8]. This theory also assumes that the wave height is considerably smaller than both the wave length and still water depth. It is important to note that linear wave theory for waves steeper than 0.01 has limitations, and potential inaccuracies may arise in simulation outputs; however, it is widely accepted in practice [9]. The potential flow on a floating body can then be described as the sum of the radiated, diffracted, and incident potential functions. These assumptions and linearization allow for $F(t)$ to be represented as a superposition of forces on the body:

$$\begin{aligned} F(t) = F_{exc}(t) + F_{rad}(t) + \ldots \\ + F_B(t) + F_m(t) + F_{PTO}(t) + F_{Drag}(t) \end{aligned} \tag{2}$$

The hydrodynamic and hydrostatic forces on the body are the initial three terms on the right-hand side of (2). The excitation force $F_{exc}(t)$ combines the diffraction force (resulting from the disturbance of waves by the floating body) and the incident force, expressed as the Froude–Krylov force (resulting from the pressure field of undisturbed waves) [5]. The radiation force $F_{rad}(t)$ is included as an added mass and wave damping term to describe the instantaneous impact of the bodies' own motion on the surrounding fluid. The buoyancy force $F_B(t)$ arises from the body's attempt to return to equilibrium and is related to the hydrostatic stiffness and displacement of the body. The calculation of F_{exc}, F_{rad}, and F_B depends on frequency-hydrodynamic parameters determined by boundary element method (BEM) solvers. In this study, the outputs of the BEM solver *WAMIT* [10] were used in both the *WEC-Sim* and *Gazebo* models for calculating these parameters.

This study incorporates supplementary forces acting on the body, as indicated by the final three terms on the right-hand side in (2). The mooring force $F_m(t)$ in this study is represented as a linear quasi-static mooring stiffness matrix [5], and the PTO force $F_{PTO}(t)$ results from the electro-hydraulic PTO affecting the body and is represented uniquely by each model. F_{Drag} is the viscous drag of the various bodies moving through the water, proportional to the square of the velocity.

2.1.1. WEC-Sim

Figure 2 presents the *WEC-Sim* Simulink model v5.0.1 designed for the MBARI-WEC. The device was represented as three rigid bodies: the surface buoy, the PTO housing, and the heave cone. Each body was characterized by its mass, moment of inertia, quadratic drag, and displaced volume. These values were identical to those used in the *Gazebo* model. The rigid bodies were subject to the aforementioned hydrodynamic and hydrostatic forces with the exception of the PTO housing, which was treated as a thin vertical cylinder well approximated by drag and static inertia terms. Because the simulated sea states were plane waves in the x-direction and the rigid bodies were axisymmetric, no sway, roll, or yaw motion was expected. Thus, the rigid bodies were confined to motion in three DOFs only: surge, heave, and pitch.

The MBARI-WEC PTO system was integrated as a distinct Simscape model, and its resultant force applied to a joint positioned between the surface buoy and tether. This joint operated in a single translational DOF relative to the orientation of the PTO housing. The PTO housing and heave cone were connected together by the tether assembly comprised of a string of rigid bodies connected by three joints that had stiffness and damping and were subject to quadratic drag forces. The choice of three joints represented the minimum number required to simulate a flexible cable without compromising computational speed [11].

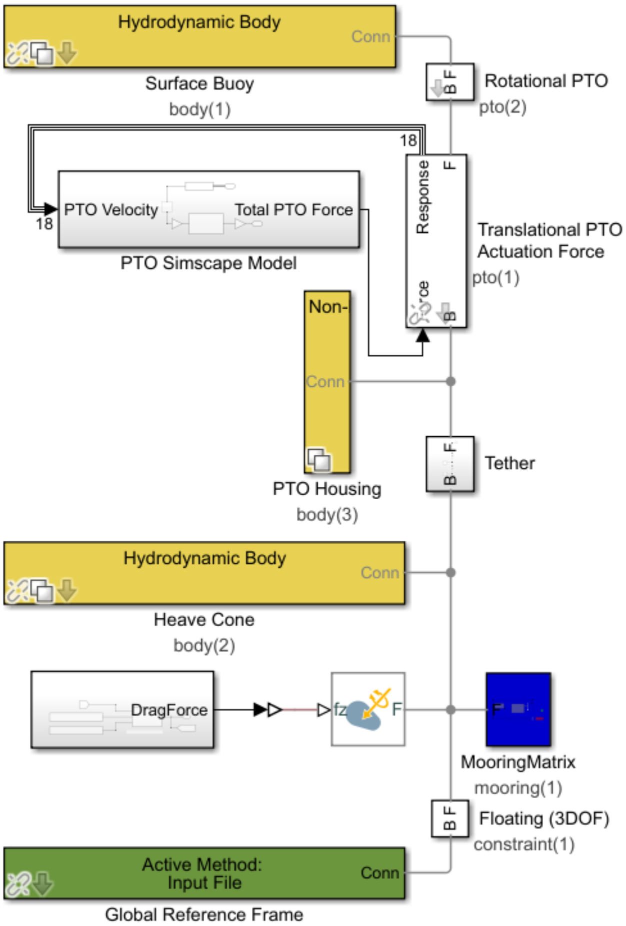

Figure 2. *WEC-Sim* model of MBARI-WEC. Labeled from top to bottom are the surface buoy, PTO (PTO Simscape model, actuation force, and housing), tether, and heave cone.

The catenary mooring system used with the MBARI-WEC was incorporated in this model as the force derived from a mooring matrix, parameterized with stiffness and damping values corresponding to each DOF, fitted from a higher-fidelity catenary mooring model as described in [3]. An additional direction-dependent quadratic drag, stemming from the asymmetric shape of the heave cone, was introduced as an external force dependent upon its heave motion. The coefficients of drag were determined from the research conducted in [3].

The *WEC-Sim* model incorporated the MBARI-WEC PTO using blocks from the Simscape library, as illustrated in Figure 3. The model was compartmentalized into distinct subsystems for the PTO, including air spring, piston, hydraulic, electric, friction, and controller feedback. The model's input parameters were derived from the work presented in [4], in which the Simulink PTO model was developed and validated against the physical PTO through experimental bench testing. In the PTO subsystem, the system took the PTO piston velocity, denoted as "PTO Velocity", as an input, and the resultant force was the output, referred to as "Total PTO Force". These variables are also illustrated in Figure 2, where they interact with the hydrodynamic model. The MBARI-WEC power electronics included a 4-quadrant driver with field-oriented control that related motor speed to torque by a default damping relationship:

$$\begin{aligned} \text{Speed [RPM]} &= [0, 300, 600, 1000, 1700, 4400, 6790] \\ \text{Torque [Nm]} &= [0, 0, 0.8, 2.9, 5.6, 9.8, 16.6] \end{aligned} \tag{3}$$

The torque could be adjusted further by a scaling factor ranging from 0.5 to 1.6 depending on sea state conditions. Moreover, when the piston retracted, characterized in this context as a positive motor speed, the torque was reduced by an additional factor of 0.6. The motor driver default damping relationship as outlined in (3) is evident in Figure 3, where "Electric Motor Torque" is correlated with "Motor Speed" through an external function.

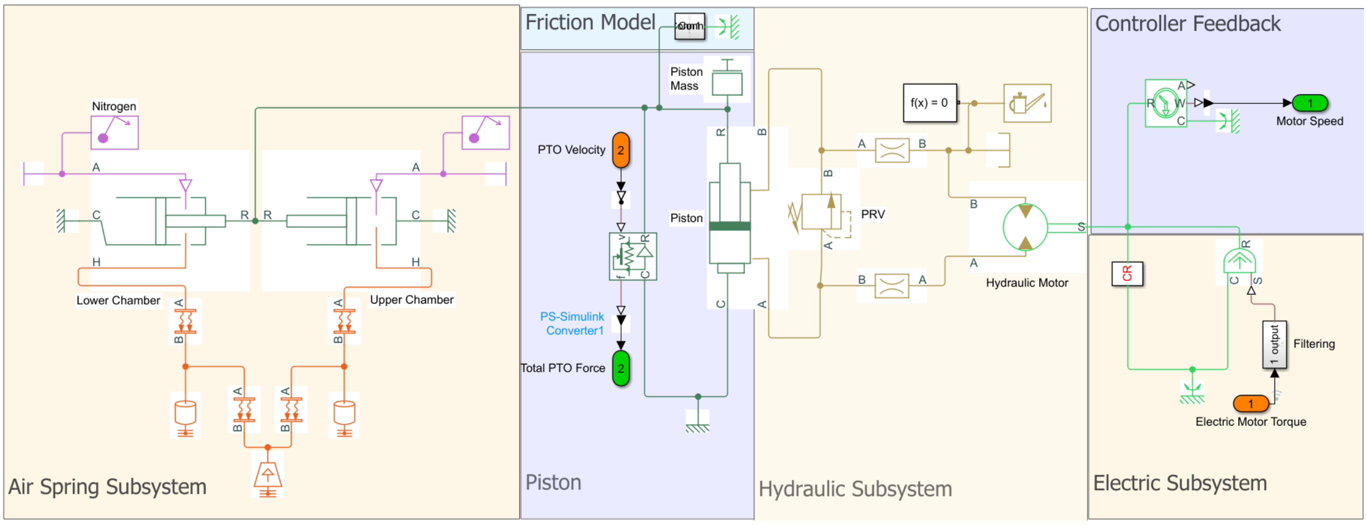

Figure 3. Simscape model of MBARI-WEC PTO. The different subsystems of the PTO are air spring, piston, hydraulic, electric, friction, and controller feedback. The orange ports are inputs and the green ports are outputs of the overall PTO system. Comparing to Figure 2, the Simulink PTO model takes in "PTO Velocity" and outputs "Total PTO Force" to interact with the hydrodynamic model. The input "Electric Motor Torque" is determined by controller feedback and dependent on "Motor Speed".

Some features within the PTO subsystems were similar in both the *WEC-Sim* and *Gazebo* models. These included the piston rod friction model and the motor friction loss model (established through bench tests) (see [4]). Key differences between the *WEC-Sim* and *Gazebo* models were how the air spring dynamics were modeled, efficiencies concerning the hydraulic motor, and the computation of electrical losses. In *WEC-Sim*, the pressure, volume, and temperature for nitrogen in each chamber of the air spring followed the ideal gas law:

$$P\,V = n\,R\,T, \tag{4}$$

where P [Pa] is the gas pressure, V [m^3] is the volume, n is the mass of the gas [kg], R [J/(kg K)] is the ideal gas constant ($R_{nitrogen} = 296.8$ [J/(kg K)]), and T is the absolute temperature [K]. Spring forces were modeled with heat transfer between the chambers and the surroundings using the energy balance equation for a closed system [4].

$$\Delta U = Q - W \tag{5}$$

$$\dot{Q}_i = K_i\,(T_{amb} - T_i) \tag{6}$$

Here, ΔU [J] is the change in internal energy, Q [J] the heat supplied or taken from the system, and W [J] the work done by the system, in this case, pressure–volume work related to the expansion or contraction of the gas spring piston. In (6), $\dot{Q}_i$ [W] is the rate of heat transfer, T_{amb} the ambient temperature (283.15 K), T_i [K] the chamber temperature, and K_i

the heat transfer coefficient (determined in [4] by fitting the model to experimental data), where the subscript i denotes either the lower or upper chamber.

Volumetric and mechanical efficiencies for the hydraulic motor were input to the *WEC-Sim* model in tabulated form provided by the manufacturer as a function of pressure drop and motor speed. Finally, the calculation of electrical losses in *WEC-Sim* were based on the PTO validation bench testing conducted in [4]. These values were provided to the model in tabulated form characterized by the motor shaft torque and speed.

2.1.2. Gazebo

The *Gazebo* MBARI-WEC model v1.1.0 [2] used in this study modeled the MBARI-WEC as four rigid bodies plus a tether assembly and is portrayed in Figure 1. One rigid body was the surface buoy which floated on the water surface and was excited by wave action. The PTO device was modeled as two rigid bodies, a larger one that was the size of the main PTO housing and another that was the contained piston which could slide in a single-DOF joint relative to the PTO housing. This joint was subject to pneumatic, hydraulic, and friction forces. The fourth rigid body of the system was the heave cone which hung below the PTO and was connected to the end of the piston by a tether assembly. The heave cone was subject to gravity and hydrodynamic forcing resulting from its motion through the water, which was presumed to be otherwise still at the depth of the heave cone. The tether was modeled as a collection of “sausage-link” rigid bodies that were connected end-to-end with rotational joints that imposed some stiffness and damping. A mooring system was not included in the *Gazebo* version used to produce the results in this study.

Each rigid body was characterized by its mass and moment of inertia matrix, as well as an added-mass matrix that depended on each body’s shape. Each body was free to move with six degrees of freedom, limited by the constraints imposed by the joints that connected the rigid bodies. Again, since the system was typically excited by plane progressive waves, often, only three degrees of motion were excited (surge, heave, and pitch), but waves not aligned with the x- or y- directions would induce more modes of motion. In addition to the inertial forces acting on the bodies due to their mass, mass distribution, and added-mass characteristics, external forces and forces between the rigid bodies completed the model. Wave forces were only applied to the surface buoy and were modeled using linear wave theory as described above. For this *Gazebo* model, the wave forcing was computed using a C++ library developed for this purpose that implements efficient computation of the time-domain wave forcing within the fixed-time-step *Gazebo* solver [12]. Buoyancy forces on the surface buoy were also computed by this library using linear wave theory.

Buoyancy forces for the fully submerged rigid bodies (PTO, piston, and the heave cone) along with the viscous drag forces for the rigid bodies were computed by a hydrodynamic forcing plugin that is distributed as part of *Gazebo*. In contrast to the *WEC-Sim* model, the drag forces on the heave cone were symmetrical: they did not depend on the direction of vertical motion of the heave cone. As shown in the *WEC-Sim* work [3], this was an approximation as the heave cone drag did in fact have some dependence on vertical direction of motion. Also note that because the PTO piston was entirely enclosed within the PTO housing, no hydrodynamic or buoyancy forces were applied to that rigid body. This resulted in a small amount of buoyancy that was neglected when the piston was extended outside of the PTO housing, but this was considered to be a negligible effect.

Like *WEC-Sim*, the piston rod friction and mechanical losses of the motor torque friction in *Gazebo* were based on models developed during the PTO bench tests [4]. *Gazebo* also implemented the motor driver default damping relationship described by (3), similarly to *WEC-Sim*. In the air spring chambers, pressure, volume, and temperature of nitrogen also followed the ideal gas law (4), but unlike *WEC-Sim*, spring forces were largely modeled using a polytropic process [2]:

$$P = P_0 \left(\frac{V_0}{V} \right)^n \tag{7}$$

where P [Pa] is the gas pressure, V [m^3] the volume, and polytropic indices $n = n_1, n_2$ represent compression and expansion behavior (determined using a linear regression of the measured pressure vs. volume curves). However, when the piston velocity was slow, the spring forces were modeled with a heat transfer model using Newton's law of cooling [2].

In contrast to the *WEC-Sim* model, the determination of volumetric efficiencies for the hydraulic motor in *Gazebo* involved an additional tuning step in which simulated and measured differences were minimized in the relationship between motor speed and piston velocity [4]. Similarly, mechanical efficiencies were determined by comparing simulated and measured hydraulic pressure versus piston force. In this case, it was found that constant efficiency values rather than manufacturer-supplied efficiency tables (as employed in the *WEC-Sim* model) yielded comparable results with the measured data. Moreover, simulations in *Gazebo* found that this approach significantly reduced simulation time. In the *Gazebo* model, computation of electrical losses incorporated both switching losses and copper losses, calculated at each time step.

2.2. Simulation Inputs

In Section 3, comparisons between outputs from the *WEC-Sim* and *Gazebo* model, and the corresponding field data from the physical MBARI-WEC, are presented for multiple observations. For a meaningful comparison between simulation and field data, it is essential to define crucial simulation parameters that accurately represent the operational state of the MBARI-WEC during each specific observation. These include the following:

1. Wave spectrum to be simulated;
2. Controller feedback scale factor;
3. Status of the heave cone doors;
4. Initial mean piston position and air spring initial pressures.

These parameters were obtained via a Sofar Spotter buoy and data being reported from the MBARI-WEC itself.

2.2.1. Sea State Spectrum

A Sofar Spotter buoy deployed near the MBARI-WEC logged data every hour. An example of a spectrum measured by the Spotter buoy on 16 September 2022 at 19:31:18 PST with a significant wave height (H_s) of 1.6 m and peak period (T_p) of 5.7 s is shown in Figure 4. Fifty-six such observations were selected; a grid showing the significant wave height and peak period of these selected conditions is shown in Figure 5.

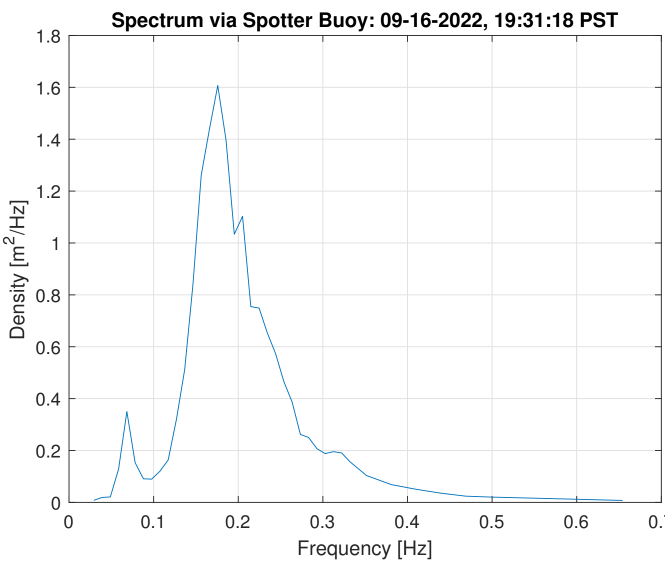

Figure 4. Example spectrum used for the simulation depicting ocean spectra for the date 16 September 2022 at 19:31:18 PST, obtained via Sofar Spotter Buoy data.

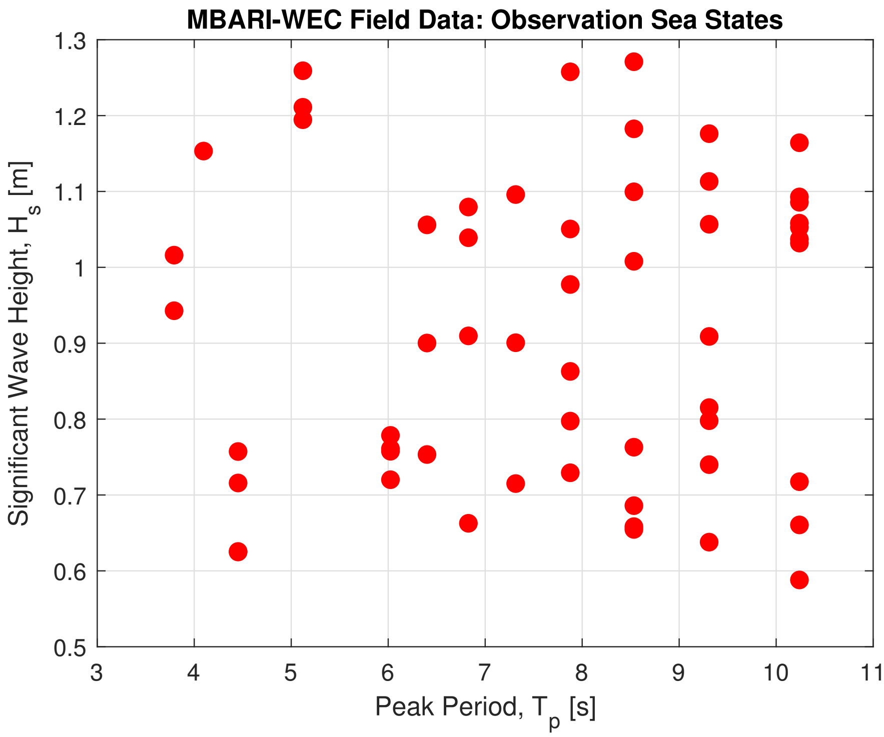

Figure 5. Sea states for each MBARI-WEC observation considered in the study.

In the statistical analysis section of the paper, the significant wave height and peak period of each observation serve as the sea state condition for a set of simulations. Each sea state was simulated using multiple phase realizations to account for non-linearities present in the model. Five simulations, each lasting five minutes for a total of 25 min of simulation, proved adequate to yield consistent statistical outcomes.

2.2.2. Controller Scale Factor

As explained in Section 2.1.1, the motor driver regulated the motor's electromagnetic torque according to (3) and subsequently adjusted it by a factor ranging from 0.5 to 1.6. Within the ROS 2 system onboard the MBARI-WEC, this factor is referred to as the *sale factor*. The scale factor used in simulating each sea state was selected by reviewing the recorded data of the MBARI-WEC.

2.2.3. Heave Cone Door Status

Depending on the sea state, the PTO piston's position could prompt a micro-controller to either open or close the heave cone doors, influencing the system's survivability by mitigating drag. The doors were programmed to open when the piston stroke exceeded 80% of its total stroke and close upon receiving a command from shore. The status of the doors was selected by reviewing the recorded data of the MBARI-WEC. Because power generation was the main focus of this paper (rather than extreme responses), only closed-door scenarios were simulated. Hence, field data observation dates and time intervals were selected to represent this condition.

2.2.4. Initial Mean Piston Position and Air Spring Initial Pressures

In *WEC-Sim*, the piston subsystem requires an initial value for the starting position. Similarly, the air spring subsystem requires values for the piston position and pressure. In *Gazebo*, these initial conditions are also mandatory and are documented in a startup batch file. In this study, the initial value was selected as the mean of the MBARI-WEC experimentally reported piston position during the considered observation and was the expected mean piston position throughout the simulation. In *WEC-Sim*, initial pressures were pre-determined and kept the piston in the middle of the stroke length during a no-wave condition. *Gazebo* utilized initial conditions derived empirically from pressure/volume curves, as described in Section 2.1.2.

3. Results

This section is split into two analyses: one in the time domain and another utilizes statistical measures. The time-domain analysis served as a direct comparison between the outputs of the *WEC-Sim* and *Gazebo* numerical models when subject to monochromatic waves. Because phase information was not available for the field measurements, statistical analyses were performed to assess the accuracy of each model against field measurements. The variables considered for this comparison were as follows:

- **Piston position [m]:** position of the PTO piston, where 0 equates to fully retracted and 2.03 equates to fully extended
- **Piston velocity [m/s]:** velocity of the PTO piston
- **Motor speed [RPM]:** speed of both the hydraulic and electric motor (directly coupled)
- **Electric power [W]:** the sum of the power to the battery and load dump; this is calculated in both models as

$$P_{elec} = P_{mech} - P_{loss,tot} \tag{8}$$

$$P_{elec} = P_{mech} - (P_{loss,mech} + P_{loss,elec}), \tag{9}$$

where P_{mech} is the mechanical power (motor torque times motor speed), $P_{loss,mech}$ is the motor mechanical power loss (motor torque friction), and $P_{loss,elec}$ is the motor electrical power losses as described in Section 2 for both models.

3.1. Time-Domain Analysis

Subjecting both the *WEC-Sim* and *Gazebo* model to the same monochromatic waves allowed for a direct comparison of their behavior. Each model was run with monochromatic waves varying from 0.25 to 2.0 m wave heights and 4 to 14 s wave periods, a scale factor of 1.0 (as discussed in Section 2.2.2), a closed heave cone door status, and a 0.8 m initial mean piston position. The top portion of Figure 6 shows the time signals for the piston position and velocity, motor speed, and electric power output by the *WEC-Sim* and *Gazebo* models when subject to a monochromatic wave with a height of 1 m and period of 8 s close to the resonance frequency of the heave cone [3]. For a non-resonant case, the bottom of Figure 6 shows these same signals when the models were subject to a monochromatic wave with a height of 1 m and period of 6 s. Table 1 shows statistical measures for the time signals in each wave case to provide quantitative measures for comparison.

Table 1. Statistical measurements for monochromatic wave time signals in Figure 6 for *Gazebo* and *WEC-Sim* models.

Wave Case		Mean Piston pos. [m]		RMS Piston vel. [m/s]		RMS Motor Speed [RPM]		Mean Electric pow. [W]	
(H, T)		Gazebo	WEC-Sim	Gazebo	WEC-Sim	Gazebo	WEC-Sim	Gazebo	WEC-Sim
1 m	8 s	0.76	0.82	0.06	0.06	648	663	32.5	2.7
1 m	6 s	0.7	0.73	0.09	0.11	1059	1247	221	291

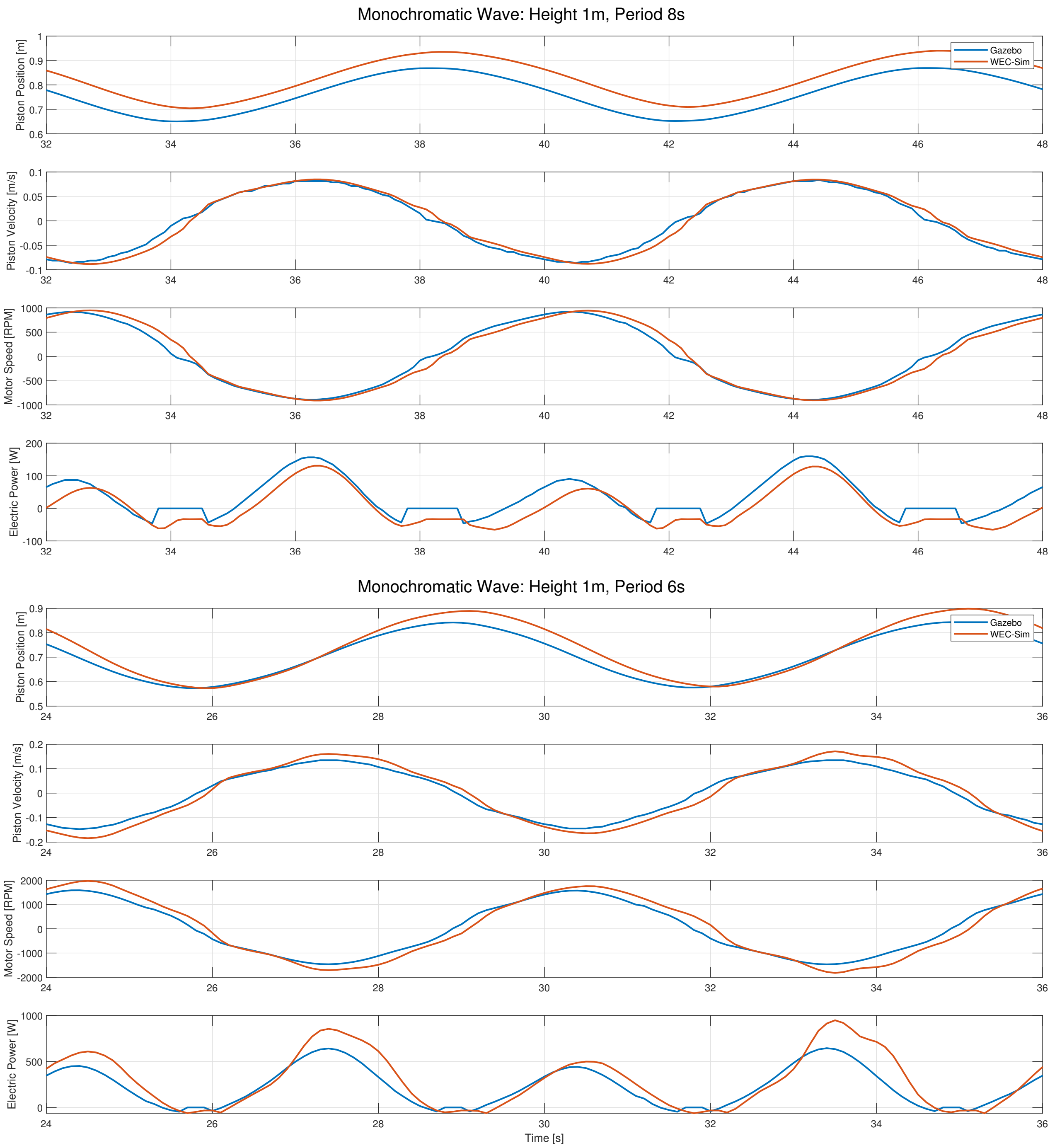

Figure 6. Time signals for piston position and velocity, motor speed, and electric power for *WEC-Sim* and *Gazebo* models when subject to two monochromatic waves (top: $H = 1\,\text{m}$, $T = 8\,\text{s}$; bottom: $H = 1\,\text{m}$, $T = 6\,\text{s}$). Both models generally exhibit similar dynamics for piston velocity and motor speed, signifying both models' insensitivity to spring stiffness despite modeling unique spring behavior.

As described in Section 2, a key difference between the *WEC-Sim* and *Gazebo* models is their approaches to modeling the dynamics of the air spring. These effects are illustrated in Figure 6. For each wave case, the differences in piston position highlighted the varying spring stiffness between the models. However, the time signals of the piston velocity and motor speed between both models largely agreed, indicating that these dynamics were not significantly influenced by spring stiffness. Studying the quantitative measurements between both models in Table 1 revealed that *WEC-Sim* maintained a closer mean piston position value to the desired value of 0.8 m. It also showed that the RMS value of piston velocity and motor speed between both models were in close agreement. The time signal of the electric power output in both models generally exhibited a similar pattern, with negative power values resulting from loss calculations. It was also noted that the electric power for both models was lower during piston retraction (positive motor speed) due to the 60% reduction in winding current that was imposed as mentioned in Section 2.1.1.

Figure 7 provides a detailed examination of the electric power, plotting it against motor speed from data obtained in the 1 m, 6 s monochromatic wave case. Both the *Gazebo* and *WEC-Sim* models showed similar dependence with motor speed, an expected result as they employed the same control algorithm.

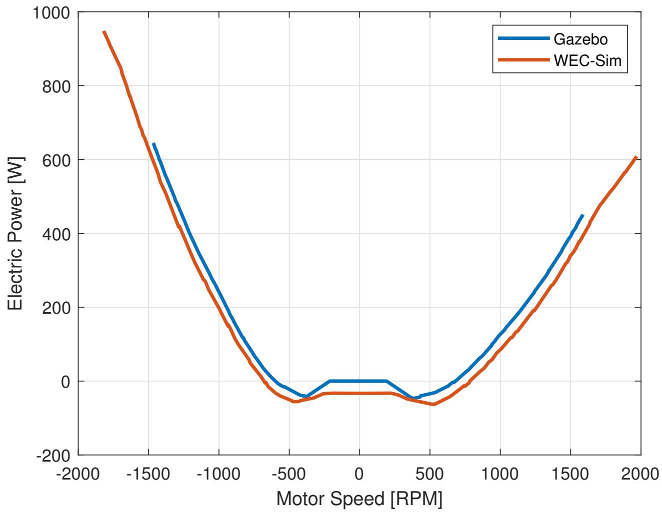

Figure 7. Electric power versus motor speed for both *Gazebo* and *WEC-Sim* models in a monochromatic wave with a height of 1 m and period of 6 s. Both models' electric power show similar dependence on motor speed except for speeds around $+/-300$ RPM. This deviation can be attributed to the utilization of PTO bench testing results [4] for power loss calculations or direct calculations using RMS current, which is dependent on speed.

3.2. Statistical Analysis

This section analyzes *WEC-Sim*, *Gazebo*, and MBARI-WEC field data measurements using statistical metrics (field measurements used in this analysis are available online at https://mhkdr.openei.org/submissions/530). As stated through Section 2.2, each numerical model used parameters based on the MBARI-WEC's operating state for each set of sea state conditions during field trials. During MBARI-WEC operation, the scale factor and status of the heave cone doors could change due to commands from shore or automated safeguards. Therefore, when selecting the time interval for observing field data used in these comparisons, cases examined in this study were chosen such that both of these variables remained constant to ensure accuracy in the comparison between field data and simulations. Time intervals varied between 30 to 60 min for all chosen field data cases.

Figure 8 compares predictions from the *Gazebo* and *WEC-Sim* models with field data for the RMS piston velocity, RMS motor speed, and mean electric power based on 56 independent observations. In each plot, the field measurements are shown on the x-axis, and simulation data are shown on the y-axis; the gray line with a slope of unity represents perfect agreement between the models and field measurements. A linear regression model was also fit to the data produced by both numerical models, and the coefficient of determination (R^2) is provided to demonstrate the degree to which the linear model accurately represents the simulation data. Visually inspecting the data for each model and their linear fit lines in all three plots of Figure 8 revealed that both models generally overestimated system performance. Studying the slope of the linear fit equations provided more information on the behavior of the simulation data as the field data parameter increased.

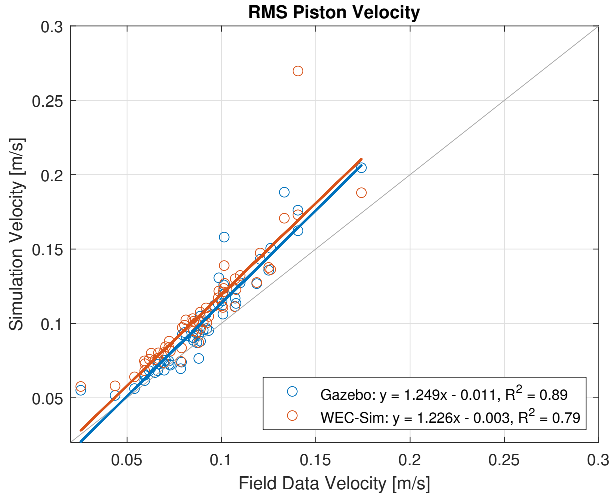

(**a**)

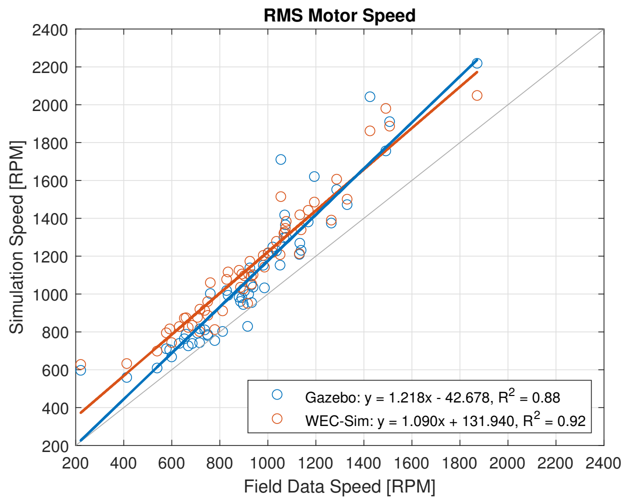

(**b**)

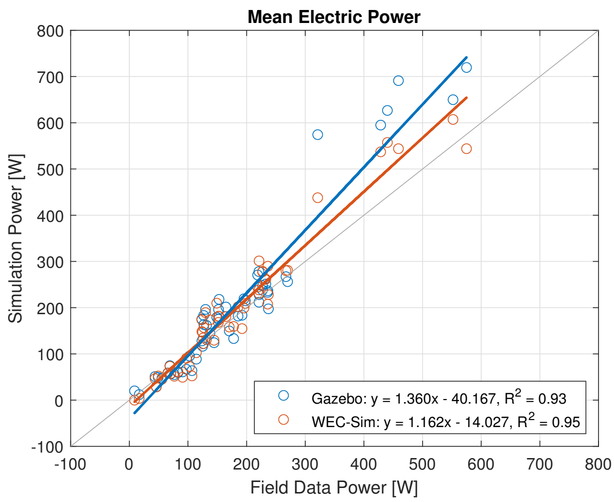

(**c**)

Figure 8. *Gazebo* and *WEC-Sim* data vs. field data for (**a**) RMS piston velocity, (**b**) RMS motor speed, and (**c**) mean electric power. The gray line with unity slope represents perfect agreement between simulation and field data. Furthermore, linear regression models were fitted for both models.

Notably, the results from *Gazebo* trended away from the field observations as magnitude increased at a higher rate than *WEC-Sim*. Typically, larger values of velocity, speed, and power occurred during more energetic sea states. The trendlines throughout Figure 8 suggested that the *Gazebo* model estimated system performance well for lower energy sea states and *WEC-Sim* did so for higher energy sea states. The sea states corresponding to these data points can be viewed by the black dots in Figure 9. Figure 9 also depicts the difference between the mean electric power of simulation data and field data binned by significant wave height and peak period, where the value represented in each bin is the average for all observations within that bin. For example, the 240 W difference in the *Gazebo* model's 0.9–1.1 m, 3.0–5.0 s bin is the average of the mean electric power differences for the two data points in that bin.

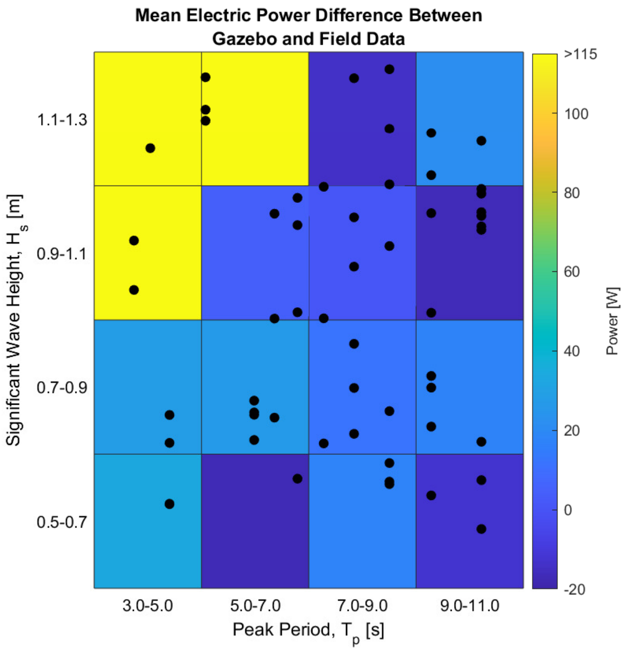

(**a**)

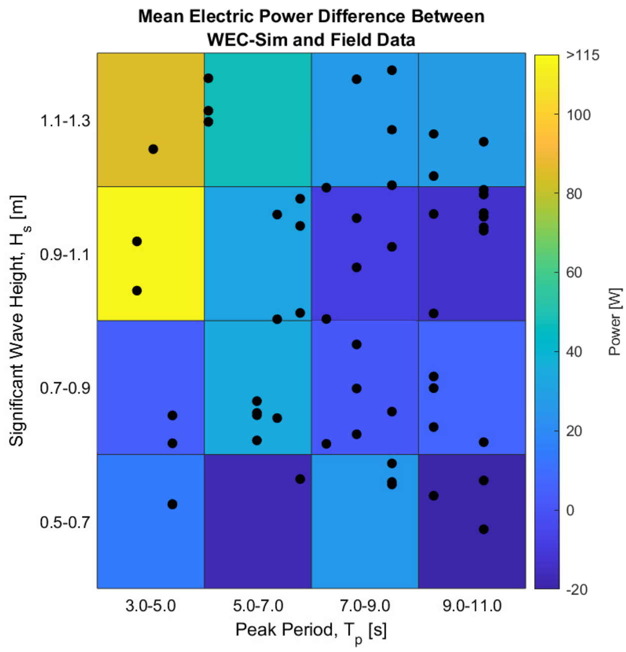

(**b**)

Figure 9. Mean electric power difference between *Gazebo*, *WEC-Sim*, and field data, binned by H_s and T_p. Black dots represent observations and their corresponding H_s and T_p value. Both (**a**) *Gazebo* and (**b**) *WEC-Sim* have less than 30 W difference except for high energy sea states where the error is between 140 to 240 W for *Gazebo* and 80 to 115 W for *WEC-Sim*.

4. Discussion

This paper analyzed two numerical models of the MBARI-WEC, one created in *Gazebo* using ROS 2 and another in *WEC-Sim* using MATLAB/Simulink, and how they compared to both each other and in representing the logged data of the physical MBARI-WEC.

Time-domain analyses with monochromatic waves uncovered similar dynamics between the models even though they employed distinct representations of the air spring in the WEC's PTO system. This suggests that the spring stiffness had minimal impact on the overall system performance. The time signal and calculated mean of electrical power emphasized each model's different computational methods for electrical losses. Figure 7 revealed that *Gazebo* computed higher power values than *WEC-Sim* for the same speed, underscoring their distinct approaches to calculating electric power loss. This was easily seen in the speed ranges between +/−300 RPM. In the damping relationship outlined in (3), these speed values correspond to 0 Nm, or equivalently, 0 Arms, resulting in no mechanical power generation. Thus, the calculated electric power was entirely due to the motor torque friction and electrical power losses. Using the equation in [4] for these speed ranges, the motor torque friction resulted in a roughly 3 W loss for both models. For electrical losses, *Gazebo*'s computation relied on the RMS motor winding current, which, as previously explained, was 0 Arms within these speed ranges, yielding zero electrical losses. Therefore, *Gazebo*'s electrical power was roughly negative 3 W, resulting solely from motor torque friction losses. However, for *WEC-Sim*, the research performed in [4] revealed that these speed ranges, along with their corresponding torque, resulted in an electric power loss of approximately 30 W, a significant difference from *Gazebo*. Furthermore, the figure explained the substantial difference between the mean electrical power of *Gazebo* and *WEC-Sim* in the 1 m, 8 s monochromatic wave case, as indicated in Table 1, since *WEC-Sim* incurred higher losses than *Gazebo* for the same speeds.

A statistical analysis was used to investigate the accuracy of each model's outputs compared to MBARI-WEC field data. While both models overestimated system performance when compared with the field observations, *WEC-Sim* tended to provide more accurate estimates for observations with high-energy sea states compared to *Gazebo*. In contrast, *Gazebo* demonstrated better predictions for low-energy sea states. While the *Gazebo* model's outputs eventually deviated from the field observations at a more pronounced rate than *WEC-Sim* in higher-amplitude cases, it provided a better estimation for a majority of the data points in the field data set. This was evident from the position of the intersection between the linear fit models in comparison to the cluster of data points when studying Figure 8. This could also be observed in Figure 9, where the sea states (black dots) available for analysis primarily had wave heights ranging from 0.5 to 1.1 m and peak periods ranging from 5 to 11 s, which are generally categorized as low-energy sea states. Therefore, the *Gazebo* model offered more accurate statistical estimates for the more frequently occurring sea states. The tendency of the *Gazebo* model to over-predict performance in the high-amplitude conditions observed in Figure 8c was also seen in Figure 9a, where agreement was within less than 30 W except for a few high-energy sea states where the error ranged from 140 to 240 W. *WEC-Sim*'s ability to predict higher-energy sea states more accurately than *Gazebo* was evident in Figure 9b, with its error ranging from 80 to 115 W for the high-energy sea states. In summary, when considering the percent difference between simulation and field data over all observations, *Gazebo* overestimated mean electric power by 12.7%, while *WEC-Sim* overestimated it by 22.2%.

The heightened agreement observed in the *Gazebo* model is likely attributed to the fact that a significant portion of its simulation parameters were finely tuned. The estimated time required to adjust the *Gazebo* parameters based on field and bench testing data was a few hours. This is in contrast to the *WEC-Sim* model, which relied more directly on data or component specifications directly obtained from the physical system bench testing or manufacturer specifications. Possible parameters that could improve the agreement of the *WEC-Sim* model with field measurements include the stiffness and damping properties of the tether setup, adding simulation buffers in the hydraulic system to aid in solving stiff equations, or including extra identified inertia in the PTO model not already represented by the Simscape blocks. Further, the results from both models revealed that the inclusion of mooring and asymmetric heave cone drag did not have a beneficial effect regarding statistical measures considered here. In the present iteration of the simulation models employed in the study, the computational time for the *WEC-Sim* model was approximately six times greater than that of the *Gazebo* model, which required roughly 1.5 min computation time per 1 min of simulation on a standard laptop.

Each of these models are well suited to different applications. The user-friendly nature and modularity of Simulink makes the *WEC-Sim* model an appealing option for quick model modifications, such as studying the effects of changing PTO piston diameter or the integration of a different hydraulic motor. Simulink tools allow for an immediate simulation analysis of multiple runs, and selecting signals for analysis is easily achieved with a simple click in the model. On the other hand, the *Gazebo* model directly replicates the control system of the actual hardware, making it an ideal platform for prototyping controllers and other algorithms before their deployment on the physical device.

Author Contributions: Conceptualization, C.D., R.C., A.H., and G.B.; methodology, C.D., D.F., A.H., and M.A; software, C.D., D.F., A.H., and M.A.; validation, C.D., D.F., A.H., and M.A.; formal analysis, C.D.; investigation, C.D.; resources, R.C., D.F., A.H., and T.B.; data curation, C.D., D.F., and A.H.; writing—original draft preparation, C.D.; writing—review and editing, R.C., D.F., A.H., T.B., and M.A.; visualization, C.D.; supervision, R.C., D.F., A.H., and T.B.; project administration, R.C. and A.H.; funding acquisition, R.C. and G.B. All authors have read and agreed to the published version of the manuscript.

Funding: This paper had funding support from the US Department of Energy's Water Power Technologies Office, grant number DE-NA0003525. They are located in Washington, DC, USA.

Data Availability Statement: Field measurements used in this analysis are available online at https://mhkdr.openei.org/submissions/530.

Acknowledgments: This work was supported by the US Department of Energy's Water Power Technologies Office. Sandia National Laboratories is a multi-mission laboratory managed and operated by National Technology and Engineering Solutions of Sandia, LLC., a wholly owned subsidiary of Honeywell International, Inc., for the U.S. Department of Energy's National Nuclear Security Administration under contract DE-NA0003525. This paper describes objective technical results and analysis. Any subjective views or opinions that might be expressed in the paper do not necessarily represent the views of the U.S. Department of Energy or the United States Government.

Conflicts of Interest: The authors declare no conflicts of interest. The funders had no role in the design of the study; in the collection, analyses, or interpretation of data; in the writing of the manuscript; or in the decision to publish the results.

Abbreviations

The following abbreviations are used in this manuscript:

MBARI-WEC	Monterey Bay Aquarium Research Institute Wave Energy Converter
PTO	Power take-off
WEC-Sim	Wave Energy Converter Simulator
ROS	Robotic Operating System
DOF	Degree of freedom
RMS	Root mean square

References

1. Atcheson, M.; Hüffmeier, J. WEC Modelling: Verification and Validation. 2019. Available online: https://www.researchgate.net/publication/349605530_WEC_Modelling_Verification_and_Validation?channel=doi&linkId=6037cfe5299bf1cc26ef8cc0&showFulltext=true (accessed on 10 November 2024).
2. Hamilton, A.; Anderson, M.; Poubel, L.; Dutia, D.; Carroll, M.; Zhang, M.; McEwen, R.; Mayans, J. MBARI Wave Energy Conversion Simulation v1.1.0. 2023. Available online: https://github.com/osrf/mbari_wec (accessed on 1 December 2022).
3. Hamilton, A.; Cazenave, F.; Forbush, D.; Coe, R.G.; Bacelli, G. The MBARI-WEC: A power source for ocean sensing. *J. Ocean Eng. Mar. Energy* **2021**, *7*, 189–200. [CrossRef]
4. Giorgi, S.; Coe, R.G.; Reasoner, M.; Bacelli, G.; Forbush, D.; Jensen, S.; Hamilton, A. Wave Energy Converter Power Take-Off Modeling and Validation From Experimental Bench Tests. *IEEE J. Ocean. Eng.* **2024**, *49*, 1–28. [CrossRef]
5. Ruehl, K.; Ogden, D.; Yu, Y.; Keester, A.; Tom, N.; Forbush, D.; Leon, J.; Grasberger, J.; Husain, S. WEC-Sim v5.0.1. 2022. Available online: https://zenodo.org/records/7121186 (accessed on 1 May 2022).
6. Macenski, S.; Foote, T.; Gerkey, B.; Lalancette, C.; Woodall, W. Robot Operating System 2: Design, architecture, and uses in the wild. *Sci. Robot.* **2022**, *7*, eabm6074. [CrossRef] [PubMed]
7. Koenig, N.; Howard, A. Design and use paradigms for Gazebo, an open-source multi-robot simulator. In Proceedings of the 2004 IEEE/RSJ International Conference on Intelligent Robots and Systems (IROS) (IEEE Cat. No.04CH37566), Sendai, Japan, 28 September–2 October 2004; Volume 3, pp. 2149–2154. [CrossRef]
8. Newman, J.N. *Marine Hydrodynamics*; MIT Press: Cambridge, MA, USA, 1978.
9. Pecher, A.; Kofoed, J. *Handbook of Ocean Wave Energy*; Springer: Berlin/Heidelberg, Germany, 2017. [CrossRef]
10. WAMIT. User Manual v7. Available online: https://www.wamit.com/manual.htm (accessed on 1 May 2022).

11. Tom, N.; Ruehl, K.; Keester, A.; Forbush, D.; Ogden, D.; Leon, J.; Husain, S.; Grasberger, J.; Topper, M.B.R.; Yu, Y.H. New Developments and Capabilities Within WEC-Sim. Ocean Renewable Energy. In Proceedings of the International Conference on Offshore Mechanics and Arctic Engineering, Melbourne, Australia, 11–16 June 2023; Volume 8, p. V008T09A076. [CrossRef]
12. Hamilton, A. FreeSurfaceHydrdynamics v1.3.1. 2023. Available online: https://github.com/hamilton8415/FreeSurfaceHydrodynamics (accessed on 1 December 2022).